

PhD Research Proposal: Towards Molecular Level Design of
Nanoporous Lyotropic Liquid Crystal Membranes for Aqueous
Separations

Advisors: Michael Shirts and Richard Noble

Benjamin J. Coscia

May 16, 2019

1 State of the Art

Commercial Membranes for Small Molecule Separations

More highly selective nanoporous membranes could be useful for performing complex aqueous separations with seawater and various sources of wastewater. For example, separating sodium chloride and boron in seawater could yield potable drinking water in water scarce regions¹ while separation of organic micropollutants found in municipal and industrial wastewaters could make existing water supplies safer to drink.² These represent only a few of the diverse contaminants of water sources.^{3,4} By efficiently separating contaminants from feed solutions with highly selective membranes, it is possible to reduce the number of required membrane passes and post-treatment steps needed for a given filtration process,⁵ thus lowering energy requirements and cost. Additionally, one can extract valuable resources from the feed streams.⁶ For example, flowback water produced during hydraulic fracturing of shale formations contains dissolved species like acetate whose extraction has economic value.^{7,8}

Reverse osmosis (RO) and nanofiltration (NF) are two prevailing commercial membrane filtration processes that can be used to separate solutes on the order of 1 nm in size and smaller, including ions. Both apply hydraulic pressure to the feed solution in order to overcome osmotic pressure and force water and unfiltered components through the membrane. RO membranes are typically thin film composite with a porous mechanical support layer and a thin but dense polymer matrix active layer where separation occurs.⁹ RO separates solutes based on the solute’s ability to dissolve into and diffuse through the tortuous pathways available in the membrane’s dense active layer. RO offers high selectivity at the cost of relatively high energy requirements since one must apply hydraulic pressure on the order of 50–100 bar to the feed solution in order to achieve an economical flux.¹⁰ In contrast to RO membranes, NF membranes have explicit pores on the order of 1 nm in size. Typically, separations are achieved based on size exclusion and Donnan exclusion if the membrane’s surface has a net charge.¹¹ NF membranes require significantly less applied pressure in order to achieve solute flux comparable to RO. Unfortunately, conventional NF membrane synthesis processes, such as phase-inversion,¹² are stochastic in nature which yields pores that are polydisperse in size.⁵ Pore size polydispersity is detrimental to membrane selectivity.

The downfall of traditional RO and NF membranes can be summarized by the well-known permeability-selectivity tradeoff. Namely, it is difficult to increase the permeability of a desired molecular or atomic species, while maintaining the same retention of undesired species.⁵

Nanostructured Membranes

Nanostructured membranes attempt to overcome the permeability-selectivity tradeoff through intelligent design at the molecular level. Ultrathin-film graphene and graphene oxide membranes are an active area of research because they are atomically thick and therefore offer potential for extremely high permeability membranes.¹³ However, scalable synthesis without introducing microscopic, performance degrading defects

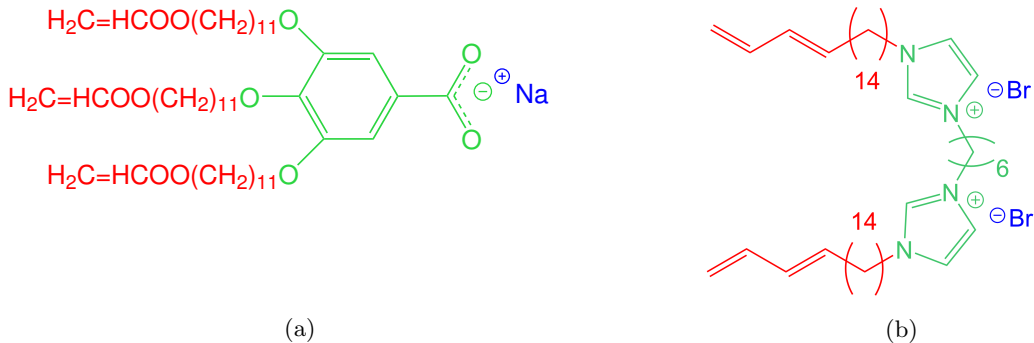


Figure 1: H_{II} and Q_I phase LLC membranes have been synthesized from monomers in (a) and (b) respectively. One can alter membrane properties by modifying the length and number of tails (red), the functional head group (green) and the counterion identity (blue) of LLC monomers.

has not yet been achieved.^{14,15} Carbon nanotubes (CNTs) have shown promise as aqueous separations membranes due to unprecedentedly fast water transport.^{13,16} Practically, dispersing and aligning CNTs into a polymer matrix is extremely difficult because they tend to agglomerate due to Van der Waals forces.¹⁷ Finally, zeolite-coated ceramic membranes offer the potential for permeabilities comparable to ultrafiltration, molecular sieves with pores up to 100 nm in size,⁵ with selectivities as good as NF and RO. A number of studies have tested the permeability and sodium salt rejection of various zeolite membranes, however none have fully overcome the permeability-selectivity tradeoff.^{18–20}

Lyotropic Liquid Crystal Membranes

Preliminary evidence has shown that cross-linked lyotropic liquid crystal (LLC) membranes can be produced at moderate scale and may be capable of performing highly selective separations.^{21,22} LLCs are amphiphilic molecules that have the ability to self-assemble into porous nanostructures²³ that can be cross-linked to create mechanically strong membrane films with periodic uniform-sized pores on the order of 1 nm in diameter.²¹ Since LLC polymer membranes have a very narrow pore size distribution, they inherently exhibit high selectivity due to their molecular weight cut-off (MWCO).²¹ Additionally, LLC monomers can be salts, and therefore lead to Donnan exclusion of ions at the membrane-feed solution interface.¹¹

The feasibility of nanostructured LLC polymer membranes for selective separations has been demonstrated using LLC monomers that form the type 1 bicontinuous cubic (Q_I)^{24–26} and the inverted hexagonal (H_{II}) phases (see Figure 1).²¹ When separating organic solutes from NaCl, Q_I-phase membrane filtration experiments have shown selectivity 2–3 times higher than commercial RO and 6–12 times higher than commercial NF membranes.⁷ When separating a series of various sized dyes, an H_{II}-phase LLC membrane showed complete rejection of dyes bigger than 1.2 nm in size.²¹

Q_I-phase membranes consist of a tortuous network of three dimensionally interconnected pores that prevent optimal through-plane transport. In contrast, the densely packed, non-tortuous and uniform sized pores of H_{II}-phase membranes represent the ideal geometry for achieving high solute flux.²⁷ However, the hexag-

onally packed LC domains of the H_{II} -phase are generally unaligned, which hurts membrane permeability. This domain scale misalignment had inhibited further development of this technology, and research efforts were focused on the Q_I phase, whose geometry does not require alignment.²²

Recently, researchers learned how to macroscopically align the hexagonal domains which has revived research into H_{II} -phase LLC polymer membranes. In 2014, Feng et al. showed that one can align Col_h domains, a temperature-dependent hexagonal phase created by neat LLC monomers, using a magnetic field with subsequent cross-linking to lock the structure in place.²⁸ In 2016, Feng et al. showed that one could also obtain the same result by confining the neat monomer between PDMS or glass substrates since hexagonal mesophases preferentially anchor perpendicular to both surfaces.²⁹

Unfortunately, reproducing the work of Feng et al. with the hydrated H_{II} phase has been an experimental challenge. Therefore, the primary focus of the most recent experimental research efforts has been on the Q_I phase.

2 Project Objectives

Our current understanding of the molecular details of LLC membranes' nanostructure is not sufficient to be able to precisely design them for specific separations. Dischinger et al. attempted to use an empirical model that correlates the physicochemical properties of the counterion used in a Q_I -phase LLC membrane to solute rejection. Although there was some agreement with their empirical model, it does not offer a sufficiently detailed explanation of the critical molecular interactions leading to the observed behavior.³⁰ H_{II} -phase LLC polymer membrane studies have been limited primarily to the Na-GA3C11 monomer (Figure 1a) with some characterization done after minor monomer structural modifications. These studies emphasized large scale structural features such as pore spacing as well as size-based rejection.^{21,31} Given the similar topology of H_{II} and Q_I membrane pores, we expect the H_{II} phase will also be subject to complex solute-membrane interactions that are not easily explained by an empirical model.

A molecular-level understanding of structure and transport in LLC polymer membranes, enabled by molecular dynamics (MD) simulations, can provide guidelines to reduce the large chemical space available to design monomers for creation of separation-specific membranes. Using a sufficiently accurate molecular model, we can observe transport of solutes within LLC membrane nanopores with atomistic resolution and infer mechanisms. Based on this information we will have a much greater capability to intelligently design new membranes by screening new liquid crystal monomer designs with MD simulations. The principles learned can be implemented and tested experimentally.

There are four primary objectives of this PhD research which are at various stages of completion.

1. Develop techniques to build and understand the nanoscopic structure of LLC membranes. (**Complete**)

A useful molecular-level model should incorporate a detailed picture of the nanoscopic pore structure, which is crucial to understanding the role of monomer structure in solute transport and membrane

design. Therefore, we must first create an atomistic model that is maximally consistent with experimental structural data. It is also necessary to evaluate and justify the minimum effort required to build systems with alternate monomers while maintaining an experimentally-consistent chemical environment.

2. Determine solute-membrane interactions that give rise to transport mechanisms. (**Complete**)

Using my most experimentally consistent configuration, I can place small molecules within the H_{II} nanopores and observe their behavior over simulation-accessible timescales. This objective aims to organize observations of various solute behaviors into distinct mechanisms that can help guide membrane design based on chemical functionality of both solutes and LLC monomers.

3. Create a stochastic model which can project long timescale transport behavior. (**In Progress**)

I will combine my qualitative knowledge of the solute transport mechanisms with simulation data in order to inform a stochastic model. This model should closely reproduce the properties of the time series that we observe in our simulations. Due to the low computational cost of a stochastic model relative to MD simulations, I will be able to forecast long timescale transport behavior and make well-converged predictions of macroscopic transport properties.

4. Adapt the analysis of Objectives 1–3 to the Q_I phase. (**In Progress**)

Over the course of this project, experimental research surrounding LLC membranes has shifted nearly all focus towards the Q_I phase due to its more facile synthesis. Although most of my work has been applied to the H_{II} phase, much of the same analyses can be applied to the Q_I phase. The biggest challenge will be adapting my techniques to its more complex three dimensional geometry.

3 Progress to Date

Objective 1: Build and understand the nanoscopic structure of the H_{II} phase (**Complete**)

My work fulfilling this objective is published in the Journal of Physical Chemistry B: Coscia et al. *J. Phys. Chem. B*, 123, 289-309 (2019).

I developed a procedure for building and equilibrating an atomistic LLC membrane system (see Figure 2). I chose to build a monoclinic unit cell consisting of four pores. Each pore is composed of monomer columns, where each column consists of 20 monomers stacked on top of each other so that the phenyl groups are coplanar with each other and the xy plane. The columns are oriented so that the hydrophilic monomer head groups face towards the pore center. I did not add any water to the initial configuration because I compared the structure to experimental data for a system claimed to be synthesized with only neat monomer.

I evaluated a number of different initial column architectures. I stacked monomers in parallel displaced and sandwiched configurations, two possible π - π stacking modes that might occur between monomer phenyl

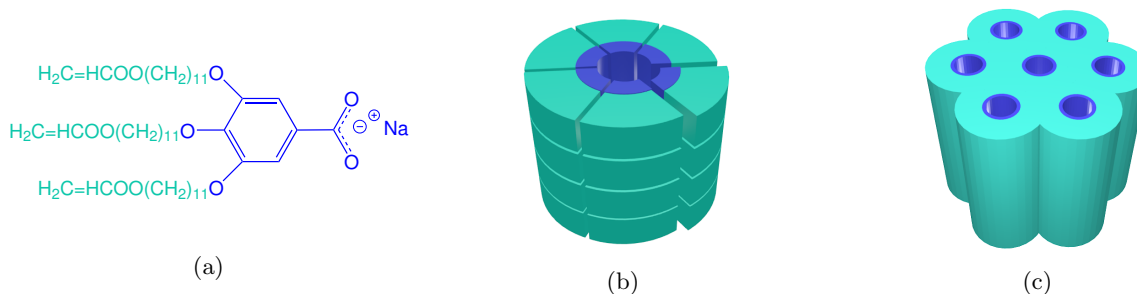


Figure 2: (a) The LLC monomer Na-GA3C11 exhibits wedge-like character. (b) Monomers stack on top of each other to create columns with short range order, then assemble into pores with hydrophilic head groups (blue) facing towards the pore center. (c) The pores assemble into hexagonally packed columnar mesophases.

groups.³² I also varied the initial distance between stacked monomers, d . I chose d values of 3.7 \AA , based on experimental WAXS measurements, as well as 5 \AA as a test of its sensitivity.

My model’s geometry is most consistent with experiment for systems built with 5 columns per pore and monomers initially stacked 3.7 \AA apart (see Figure 3). I equilibrated systems with 4, 5, 6, 7 and 8 columns per pore. The pore spacing of 5 column-per-pore systems agree well with experiment. 6 column-per-pore systems built with $d = 5 \text{ \AA}$ appear to yield an experimentally consistent pore spacing however, the equilibrated distance between stacked monomers stay close to 5 \AA which is inconsistent with experiment. In general, the equilibrated distance between monomers stays close to its initial value.

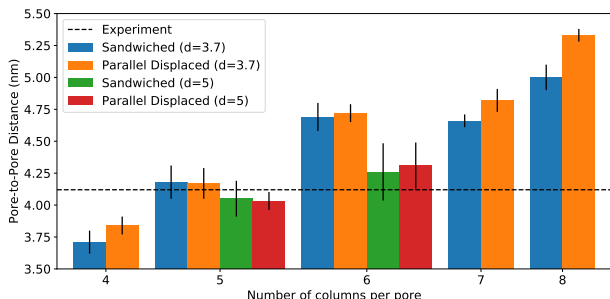


Figure 3: Systems with 5 columns per pore have equilibrated pore spacings closest to the experimental value of 4.12 nm . The equilibrated pore spacing of the model increases as the number of columns in each pore increases.

simulated to this point could reproduce R-double.

It is necessary to add a small amount of water to the model in order to fully reproduce all features of the WAXS pattern (see Figure 4b). I obtain the most experimentally consistent structure when I build systems in the parallel displaced configuration with 1 wt% water added to the pores. This is the only configuration that gives rise to the R-double feature without imposing some kind of position restraint. R-double appears because vertically adjacent monomer head groups hydrogen bond with shared water molecules, causing them to be drawn closer together. When multiple pairing interactions occur in series along the same pore axis, the center of masses of the pairs are spaced apart at twice the π -stacking distance. The necessity of water in

I further validated the structure of our molecular model by verifying its consistency with five major reflections present in the experimental WAXS pattern. Using MD trajectories, I simulated X-ray diffraction (XRD) patterns that we could compare to the WAXS data by taking the appropriate cross-section of the time-averaged 3D structure factor. The five major reflections and the structural features leading to them are summarized and described in the caption of Figure 4. Note that none of the models

my model suggests that the membrane synthesized by Feng et al.^{28,29} was slightly hydrated due to water molecules leached from surroundings by the hydroscopic monomers. Similar suspicions have been voiced by experimentalists in unpublished communications.

My model exhibits slow dynamics on timescales longer than can be reasonably simulated with current computer resources. Consequently, there are very few uncorrelated frames in the trajectories which leads to noise and sharpened reflections in the simulated XRD patterns. One can overcome this issue by combining the structure factors generated from an ensemble of simulated trajectories each produced from an ensemble of uncorrelated initial configurations. One can create decorrelated initial configurations by randomly displacing monomer columns in the z -direction.

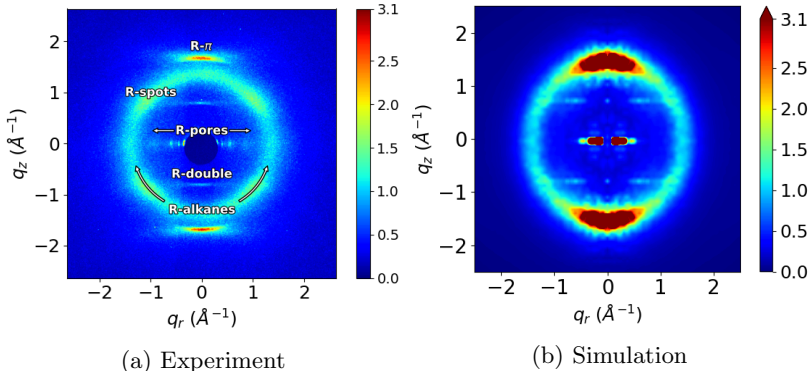


Figure 4: (a) 2D-WAXS gives details about repeating features on the order of angstroms. Explanations for each of the 5 major reflections present are as follows: (R- π) Aromatic head groups $\pi - \pi$ stack 3.7 Å apart. (R-double) Monomer head groups associate into pairs by hydrogen bonding with a shared water molecule. R-double does not appear in dry systems. (R-alkanes) Alkane chain tails pack 4.5 Å apart. (R-spots) Monomer tails pack hexagonally. (R-pores) The pores are spaced 4.12 nm apart and pack hexagonally. (b) We obtain a maximally consistent match between simulated XRD patterns and experimental WAXS data when we build systems in the parallel displaced configuration with 1 wt % water included in the pores.

Perhaps the most important conclusion from my structural work is that the chemical composition of the pores is relatively insensitive to the initial configuration. In Figure 5, I plot the radial distribution function of various monomer components as a function of distance from the closest pore center. All are qualitatively similar meaning that a solute placed in any of these systems should experience a similar chemical environment. Although we will move forward with our most promising configuration, this is an important finding since it implies that one does not need to apply the same level of rigor when screening new monomers.

Objective 2: Determine transport mechanisms (Complete)

A manuscript based on the work presented towards this objective is under review for publication in the Journal of Physical Chemistry B.

I added additional water to the most experimentally consistent structural model in order to create a higher water content H_{II} phase model. Researchers have synthesized the H_{II} phase using the NaGA3C11 monomer with water contents ranging from 7 - 20 wt%, with close to 10 wt% being the most common.^{21,23} However, Resel et al. stated that the system is likely fully hydrated at 7 wt % water with excess water trapped in defects between hexagonal mesophases.³¹ Consequently, I chose to build two systems with 5 and 10 wt% water.

Upon simulating each system, I observed that water partitions into the distal tail region. Based on the radial distance from the pore center where the minimum water density occurs, we defined the distal tail

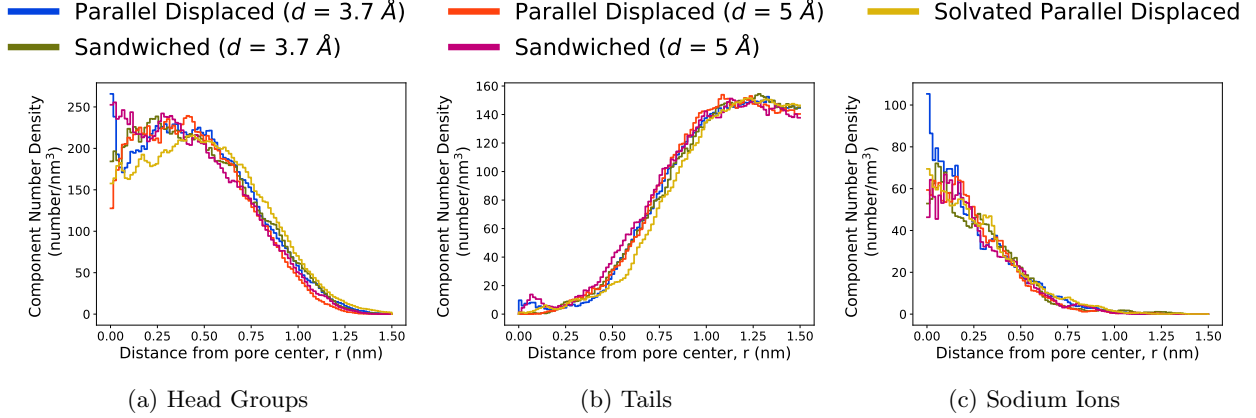


Figure 5: Even if we fail to get the system’s structure exactly right, we can still expect to extract useful transport details. In all systems studied, the component radial distribution functions are similar. They exhibit a composition gradient transitioning from the hydrophilic to the hydrophobic regions. The biggest differences are at $r=0$ where noise is higher due to decreased sampling. The center of the pore is not hollow, but contains sodium ions and head groups, even when the system is solvated. This architecture may impede transport in the real system in a chemically-dependent manner. The solvated system has a lower density of head groups near the pore center which is likely due to the swelling that is necessary in order to fit water molecules in the pore region.

region to be greater than 1.5 nm from any pore center. There is approximately a 3:2 ratio of water in the pores to water in the distal tails. Due to the wedge shape of the monomers, the distal tail region has a relatively low density leaving space for water molecules to fill.

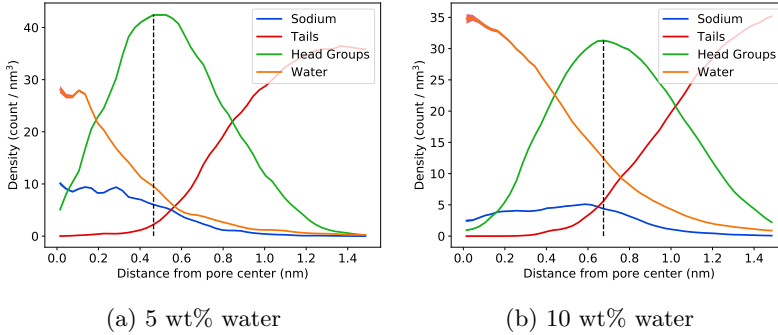


Figure 6: The radial densities of various monomer components paint a picture of the pore topology where the pore centers are primarily composed of water, sodium ions and head groups to varying degrees depending on total water composition. The monomer groups labeled in each plot correspond to the color-coded monomer pictured in Figure 1a. All RDFs represent the number of atoms located at a given distance from the pore center normalized by the volume of the annular bin to which they belong. The black dashed lines are positioned so that they intersect with the maximum head group density. (a) In the 5 wt % system, monomer head groups are situated about 0.45 nm from the pore center. Sodium and water are densest near the pore center (b) Monomers in the 10 wt % system retreat an additional 0.2 nm to make room for more water. Water is densest at the pore center, but sodium ion density peaks closer to the head groups since many stay bound to carboxylate groups.

The pores of the H_{II} phase are a mixture of water, sodium ions and monomer head groups. Water is densest at the pore center ($r = 0$). The maximum density of head groups occurs 0.45 and 0.65 nm from the pore center in the 5 and 10 wt% water systems respectively (see Figure 6).

Water and sodium transport is significantly faster in the less crowded 10 wt% water pores. The mean squared displacement (MSD) of water is about 51 times higher and the MSD of sodium is about 49 times higher compared to the 5 wt% system. In general we observe similar solute transport mechanisms in

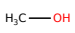
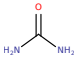
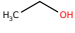
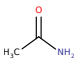
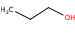
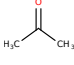
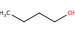
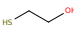
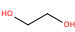
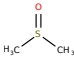
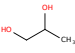
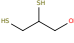
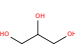
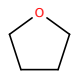
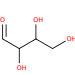
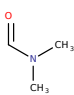
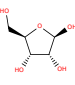
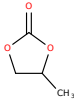
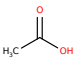
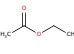
Solute Name	Abbreviation	Structure	Solute Name	Abbreviation	Structure
methanol	MeOH		urea	URE	
ethanol	EtOH		acetamide	AcN	
propanol	PrOH		acetone	ACE	
butanol	BtOH		mercaptoethanol	ME	
ethylene glycol	EG		dimethyl sulfoxide	DMSO	
propylene glycol	PG		2,3-dimercapto-1-propanol	DMP	
glycerol	GLY		tetrahydrofuran	THF	
tetrose	TET		dimethylformamide	DMF	
ribose	RIB		propylene carbonate	PC	
acetic acid	AcOH		ethyl acetate	EAC	

Figure 7: The solutes studied in this work along with the abbreviations used in subsequent figures and their chemical structures. Solute names are color-coded according to similarities in their structure. Blue corresponds to simple alcohols, red to diols, triols and sugars, green to ketone-like solutes, orange to sulfur-containing solutes and yellow to solutes that can only accept hydrogen bonds but not donate.

the 5 and 10 wt% water systems but on different time scales.

I explored the influence of a solute’s chemical functionality on its transport properties within the H_{II} nanopores. For each solute, I created a separate initial configuration and placed 6 solutes, equally spaced in z , in each nanopore. This gave a sufficient number of solute trajectories from which to generate statistics while maintaining a low degree of interaction between solutes.

The solute MSDs are not a monotonic function of solute size. In Figures 8a and 8b, we plot the average MSD of each solute. In Figure 8c and 8d, I plotted the solute MSDs against their molecular radius. Also plotted are theoretical curves which illustrate the expected MSD of each solute if they were to travel unhindered. The Stokes-Einstein equation with the correction factor of Gierer and Wirtz³³ passes through methanol’s MSD and radius in order to give an approximate frame of reference. The correction factor attempts to include the effects of microfriction that begin to play a role when solute size becomes on the order of solvent size. Since methanol is small, I assume that it travels unhindered relative to all other solutes. The theoretical line serves as an approximate boundary between subdiffusive, Brownian and superdiffusive behavior. In the majority of cases, solute MSDs fall well below the theoretical lines and therefore are subject to more hindrance than methanol due to factors other than size.

Intermittent hops between long periods of entrapment lead to subdiffusive solute transport behavior. As implied by Figures 8d and 8c, most solutes move significantly slower than expected. In Figure 9a, I've plotted the z -direction trajectory of three ethanol molecules. Typically, long periods of entrapment occur when ethanol molecules are far from the pore center, while there is a much greater degree of mobility close to the pore center. The MSD curve averaged over all ethanol trajectories is shown in Figure 9b. The curve is sub-linear and thus subdiffusive.

Due to the crowded environment among the monomer tails, solutes generally move faster in the less dense pore region. Figure 10a shows that this is the case for all solutes. Hops made in the pore region are on average 59 % larger than those made outside the pore region.

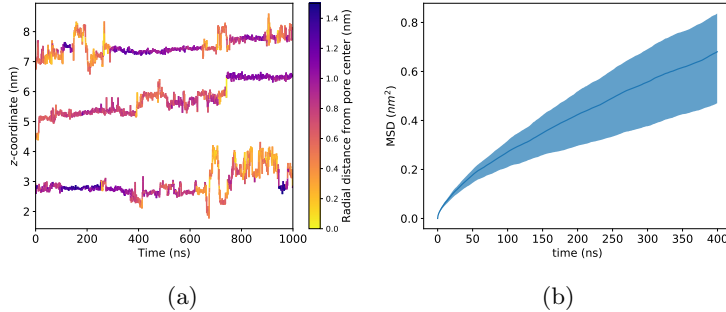


Figure 9: All solutes show subdiffusive transport behavior inside the membrane's nanopores, similar to that exhibited by ethanol. (a) The z -coordinate trace of 3 representative ethanol COMs shows clear periods of entrapment separated by hops. In general, the longest dwell times occur when solutes are situated far from the pore center and the hops occur when solutes are close to the pore center. (b) The time-averaged MSD of ethanol is sub-linear which suggests transport is governed by an anomalous subdiffusion process.

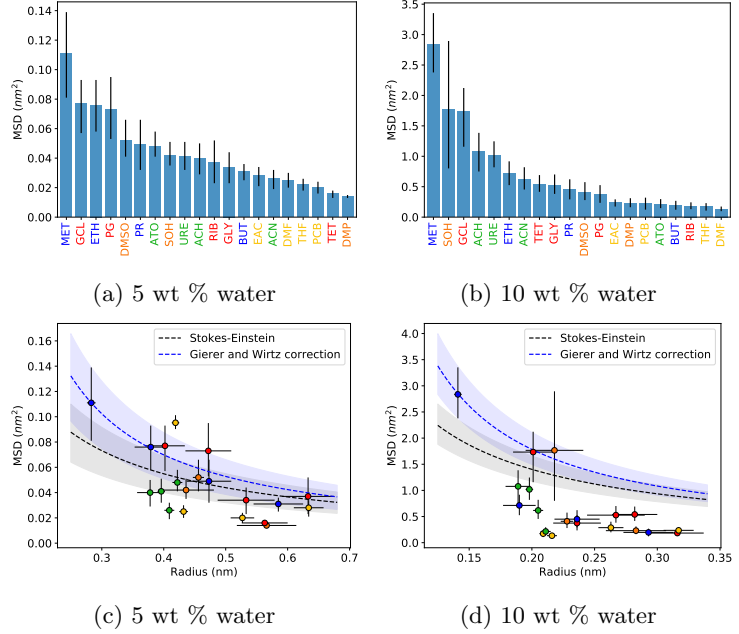


Figure 8: The MSDs of solutes in the 5 wt % water system (a) are significantly smaller than those of the solutes in the 10 wt % water system (b). The MSDs are not a monotonic function of molecular size (c and d). A significant number of solute MSDs fall below the theoretical lines predicted by the Stokes-Einstein equation and Gierer and Wirtz' corrected Stokes-Einstein equation.

However, time spent in the pore region does not necessarily result in a high MSD. For example, ribose spends the largest fraction of time in the pore region, but has the fifth lowest hop frequency and the third lowest average MSD (see Figures 10b and 10c). Therefore, proximity to the pore center cannot be the sole variable that determines transport properties.

Among the set of solutes studied, we observe three different mechanisms of entrapment that are responsible for subdiffusive behavior:

1. As already demonstrated by Figures 9a and Figure 10a, solutes that drift away from the pore center

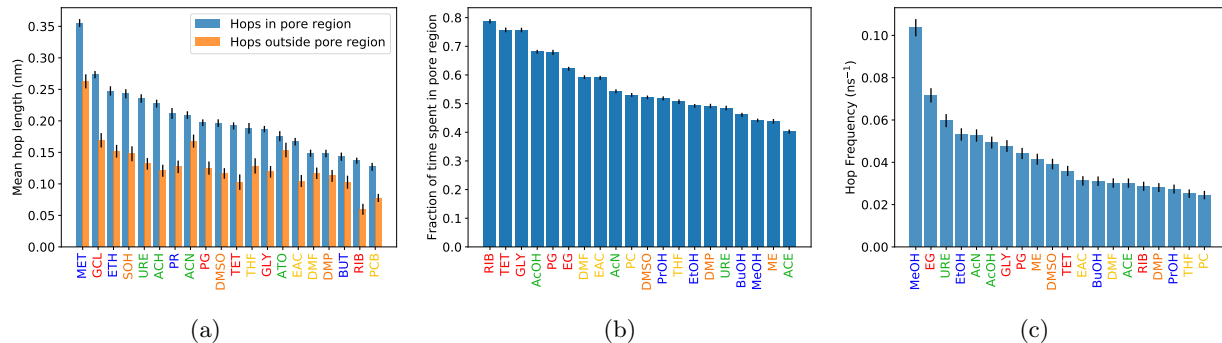


Figure 10: (a) Hops made in the pore region of the 10 wt% water system are, on average, 59 % larger than those made outside the pore region. The trend in hop lengths is similar to the trend in MSDs shown in Figure 8b implying that solutes which make consistently larger hops have higher MSDs. The fraction of time spent by a solute in the pore region (b) does not necessarily lead to more frequent hopping (c). For example, ribose spends the largest fraction of time in the pore region, yet performs the fifth lowest number of hops and third lowest MSD.

can become entangled in the monomer tails.

2. Many of the solutes we studied are capable of donating hydrogen bonds to monomer head groups and thus are prone to temporary immobilization through this interaction.
3. Because all solutes are polar, they have regions of concentrated electron density, modeled as partial charges, which can associate with sodium ions bound to monomer head groups.

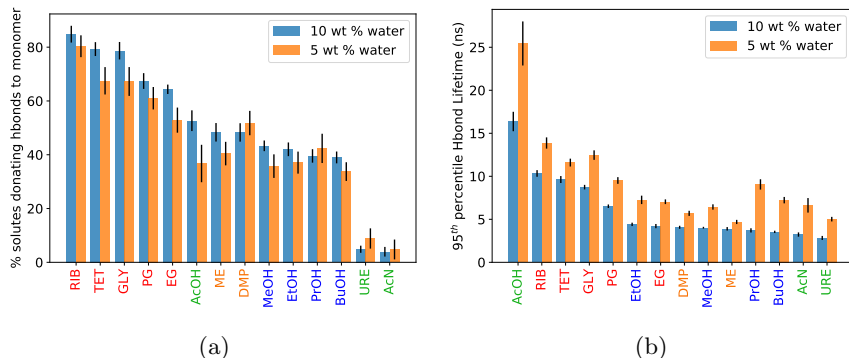


Figure 11: (a) Solute capable of donating hydrogen bonds to monomer head groups do so to varying degrees. The reported percentages represent unique solute-monomer hydrogen bonds. Individual solutes that hydrogen bond with multiple head groups simultaneously are only counted once. (b) The lifetime of individual hydrogen bonds appears correlated to the percentage of solutes involved in hydrogen bond interactions. Hydrogen bond lifetimes tend to be longer for solutes that hydrogen bond frequently. Note that solutes incapable of donating hydrogen bonds are omitted from this figure.

and glycerol, can donate multiple hydrogen bonds to monomer head groups simultaneously. When one hydrogen bond is broken, other hydrogen bonds work to hold the solute in place, which allows broken hydrogen bonds to reform. Solutes containing sulfur and nitrogen atoms in place of oxygen atoms hydrogen bond less frequently since they are less electronegative elements.³⁴ The lifetime of hydrogen bonds follows nearly the

The frequency with which solutes donate hydrogen bonds to monomer head groups is related to the number of hydrogen bond donating atoms as well as their identity. The percentage of solutes actively participating in at least one hydrogen bond with a head group each frame descends as the number of hydroxyl groups decreases (Figure 11a). Solutes with many hydroxyl groups, such as ribose, tetrose

same trend (Figure 11b). Hydrogen bonds of solutes that hydrogen bond more frequently last longer.

Solutes with carbonyl groups tend to associate with sodium ions most frequently. Nearly all of the most coordinated solutes contain a carbonyl group, except for DMSO which has an analogous sulfinyl group (see Figure 12a). There is a significant drop in sodium ion association for solutes that do not contain carbonyl groups or multiple hydroxyl

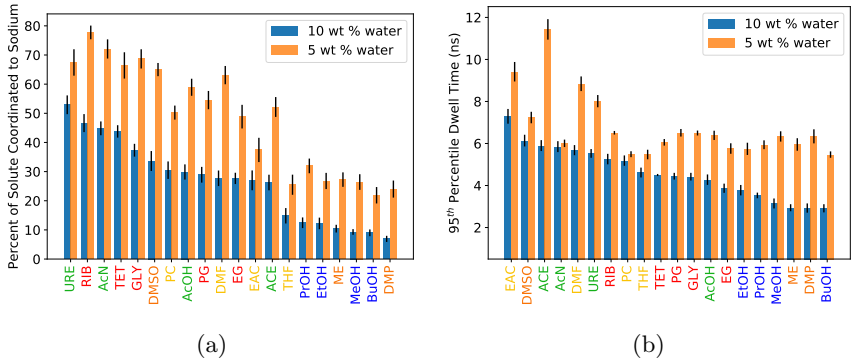


Figure 12: (a) Solutes, especially those with carbonyl groups, spend a significant fraction of time coordinated to sodium ions. (b) The length of time a solute-sodium pairs spends associated tends to be higher for pairs that associate more frequently.

groups to compensate. The corresponding dwell times follow a similar trend, however the dwell times of highly coordinated solutes with multiple hydroxyl groups are generally lower since association between hydroxyl groups and sodium is apparently a weaker interaction (Figure 12b). Solutes with nitrogen atoms adjacent to the carbonyl groups tend to associate with sodium ions significantly more.

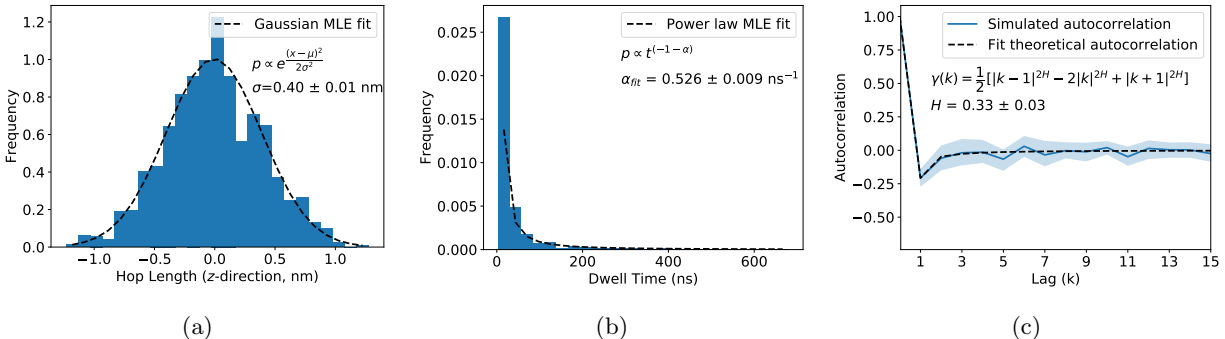


Figure 13: The movement of solutes may be well-described by an sFBM process which can be simulated using parameters that describe the solute’s hop lengths, dwell times and degree of correlation between hops. Here I use the parameters derived from ethylene glycol as an example. (a) The distribution of hop lengths made by ethylene glycol appears Gaussian, which can be described by the maximum likelihood estimate (MLE) of the σ parameter, with assumed mean, μ , of 0. (b) The distribution of dwell times between hops can be fit to a power law whose decay is described by the MLE of the parameter α . (c) Hops are anticorrelated to their previous hop as indicated by the negative value at $k = 1$ of the autocorrelation function, γ . The Hurst parameter, H , is a measure of long term memory of the hops and is directly related to the autocorrelation function of a fractional Brownian process.

Objective 3: Create a stochastic model (In Progress)

While one can clearly learn a great deal of qualitative information about mechanistic behavior on MD-accessible timescales, my work’s impact would greatly increase if I could create a model that could predict macroscopic quantities such as permeability and selectivity within a reasonable degree of certainty. A stochastic model derived from simulation data could achieve this however, there is not a well-defined procedure for

this type of extrapolation. Therefore, I am exploring two different approaches towards this end.

Approach 1: subordinated fraction Brownian motion: My first route towards a stochastic model is to simulate realizations of a subordinated fractional Brownian motion (sFBM) process based on parameters extracted from solute time series. As demonstrated by the example in Figures 13a and 13b, the distribution of hop lengths in the z -direction appear Gaussian while the distribution of dwell times between hops appears to be described by a power law. Alone, these distributions characterize a continuous time random walk (CTRW), a subdiffusive process where particles hop a random distance in a random direction and stay there for a random period of time.³⁵ Unlike a CTRW, the hops in the system I study appear anti-correlated to their previous hop as demonstrated by the autocorrelation function in Figure 13c. A CTRW with anticorrelated hops is well-described by an sFBM process.³⁶

Solute MSDs calculated based on realizations of an sFBM process mostly preserve the trends in MSD calculated directly from MD simulations (see Figure 14), but the predictions are generally too low. For each solute, I used the parameters described in Figure 13 to generate $1e4$ realizations of an sFBM process, each with the same length as the MD simulations (1000 ns) so that I could make a direct comparison between their MSDs. While the sFBM MSD prediction for methanol is too high, the rest are on average only 46% of the MD calculated MSD values.

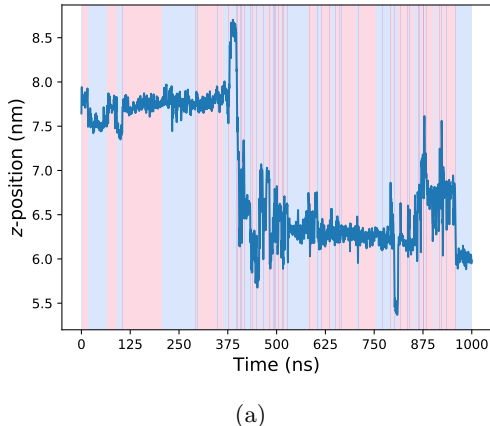


Figure 15: In order to generate the parameters used in our first approach, I identified hops based on change points in the time series, indicated by color transitions. In addition to errors in change point detection, all information between change points is lost.

If the two state model proves insufficient, I can add increasing levels of complexity. For example, I might

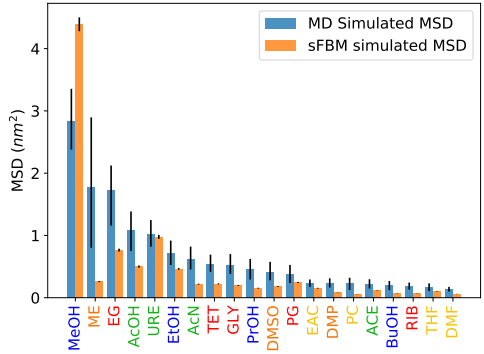


Figure 14: The trends in the MSD calculated directly from MD simulations and from realizations of the sFBM process mostly agree, but the sFBM predictions are generally far too low.

This approach might be improved by incorporating radial dependence into the three sFBM parameters described in Figure 13. In Figure 10a, we showed that hops by solutes situated inside the pores are 59% larger than hops by solutes in the tails, which leads to two distinct values of σ . Similarly, we can determine radially dependent values of α and H .

A simple two state model, in pore versus out of pore, may be sufficient to fully incorporate radially dependent effects. Based on the fraction of time spent in the pore region (Figure 10b), we can determine the appropriate balance of each type of parameter to use when simulating sFBM realizations. We would also need some kind of switching frequency, or dwell time in each region since it does not make physical sense for a solute to enter and exit the pore region every other time step.

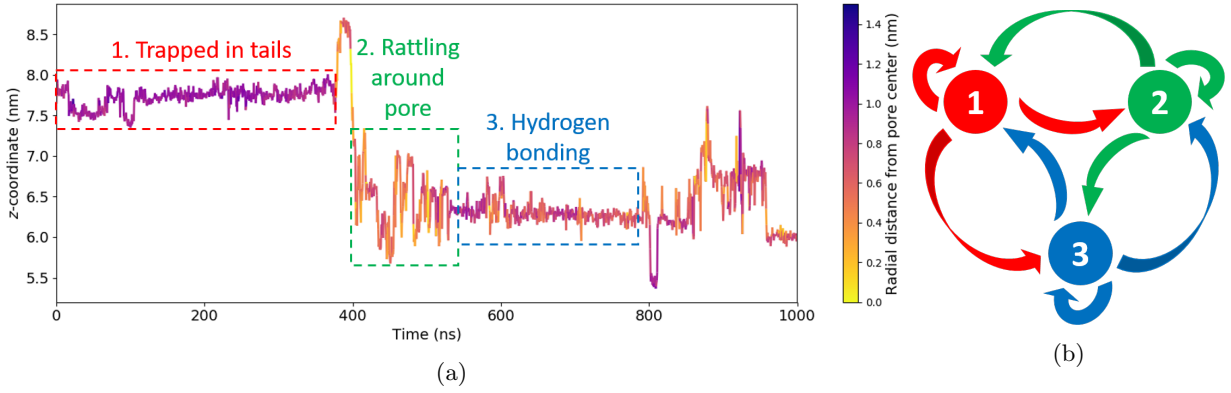


Figure 16: Using my second approach, I will be able to classify the behavior of solutes into distinct states. (a) As an example, I’ve come up with three potential states based on the time series pictured above. State 1: solutes far from the pore region are trapped in the tails leading to restricted motion. State 2: unbound solutes within the pores make large and frequent movements. State 3: solutes are held in place by hydrogen bonds with monomer head groups (b) There is a probability associated with each transition between states, represented by the arrows above. For example, following the red arrows, there are probabilities associated with going from State 1 to State 2, from State 1 to State 3 and from State 1 back to State 1.

make the radial dependence a continuous function, or I could assign parameters that are dependent on the type of trapping mechanism affecting the solute.

It is important to note that this first approach does not use a significant fraction of the data. In order to construct distributions of hop lengths and dwell times, I needed to locate precise time points at which hops occurred. I achieved this using an off-line change point detection algorithm implemented in the python package `ruptures`.³⁷ The algorithm does a decent job of identifying hops, but still loses information as demonstrated in Figure 15a.

Approach 2: Markov Switching Models: Instead of limiting my analysis to 3 fitting parameters (α , σ and H), my second approach uses all of the available data in order to classify sequences of time series behavior into distinct states. In Figure 16a, for demonstrative purposes, I’ve identified 3 potential states defined by the solute’s behavior during the time bounded by each box. Once we’ve identified states, we can use our data to define a matrix of probabilities describing switches between states, following a Markovian framework (see Figure 16b).³⁸

I will use the Kalman filter algorithm in order to identify distinct states in solute time series and simultaneously describe the dynamics of each state.³⁹ In general, the Kalman filter can attempt to linearly project subsequent steps in a time series based on its past values. The error in each prediction is stored sequentially. Regions of the time series associated with the largest prediction uncertainties can be used as an indication of a state change. Using a non-parametric Bayesian approach to identify states, I will not need to pre-define the number of states, which will allow the data to drive the model’s complexity.⁴⁰ A convenient byproduct of the Kalman filter are maximum likelihood estimates for parameters which describe the time series in terms of an autoregressive moving average (ARMA) process.⁴¹

$$Y_t = c + \phi_1 Y_{t-1} + \phi_2 Y_{t-2} + \cdots + \phi_p Y_{t-p} + \epsilon_t + \theta_1 \epsilon_{t-1} + \theta_2 \epsilon_{t-2} + \cdots + \theta_q \epsilon_{t-q} \quad (1)$$

where Y_t represents the time series value at time t , ϵ is a white noise parameter and ϕ and θ are coefficients determined by the Kalman filter. With knowledge of the transition probabilities and the dynamic behavior of each state described by Equation 1, I can forecast solute time series orders of magnitude longer than with molecular simulations.

Objective 4: *Apply analyses to Q_I phase* (In Progress)

Paralleling my work on the H_{II} phase, my first task towards this objective was to build a suitable unit cell representation of the Q_I phase. Unfortunately, the true space group of the Q_I phase that we are studying is unknown. Experimental diffraction has narrowed down the possible bicontinuous cubic configurations to the Ia3d and Pn3m space groups.⁴² Therefore, we will build both types of unit cells and search for clues that can be used to differentiate them experimentally.

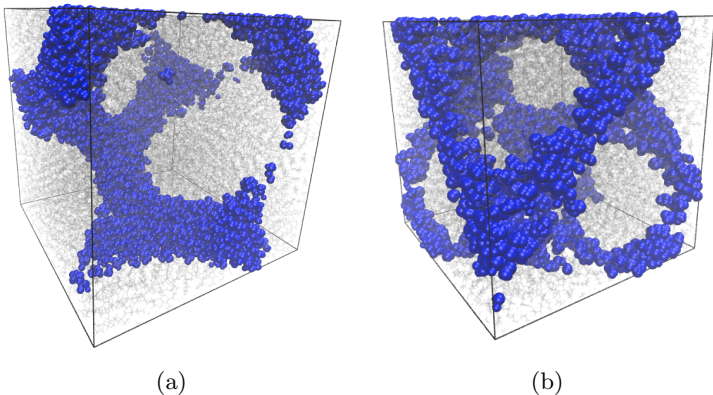


Figure 17: I developed a procedure capable of building both (a) Ia3d and (b) Pn3m unit cells from arbitrary monomers with controllable pore size. The blue glycerol molecules highlight the aqueous region where transport occurs.

I have developed a procedure that can build both Ia3d and Pn3m unit cells. To our knowledge, nobody has ever built an atomistic molecular model of a bicontinuous cubic phase system. Some systems have been created by allowing coarse grained representations to self-assemble over long timescales.⁴³ However, self-assembly can be a long process, especially for fully atomistic systems, where it might take multiple orders of magnitude longer than what we can reasonably

simulate. Instead, I use analytical equations that describe the surface of these systems in order to place monomers into a unit cell.⁴⁴ Monomers are placed perpendicular to the surface in random locations that don't overlap. One can control the pore size by translating monomers perpendicular to the surface at the point where they are attached.

First, I will study the structure of the Q_I phase using methodology similar to that used for the H_{II} phase. I will attempt to identify one of the space groups as the most likely experimental configuration based on simulated XRD signatures, although this might not work due to the known similarity of Ia3d and Pn3m XRD patterns.

Then I will study transport of solutes within these atomistic unit cells, adapting the same analyses used in Objectives 2–3. The primary challenge will be adapting my techniques to the more complex pore geometry of the Q_I phase, however I expect that the main conclusions will not deviate far from those of the H_{II} phase since the chemical environments within the nanopores are qualitatively similar.

The experimental performance of Q_I phase membranes has been studied far more extensively than that of the H_{II} phase. Therefore, I may be able to identify which space group is correct if one system exhibits

experimentally inconsistent transport properties and one does not. I can attempt to replicate the trends in the results of the separation studies performed by Dischinger et al.⁷ If I can match the experimental trends, then there is a good chance that I can use my molecular model to offer an explanation for the complex behavior described in their work (see first paragraph of Section 2).

4 Timeline for Completion of Objectives

A schematic of the estimated timeline that I plan to follow for the completion of tasks pertinent to finishing all objectives is given in Table 1. Ideally, each task will become a published manuscript. I will run simulations required to study the structure of the bicontinuous cubic phase in parallel with the continued development of my stochastic model of transport in the H_{II} phase. Simulations and analysis required for Q_I phase solute transport studies analogous to those of Objective 2 will be carried out throughout Fall 2019. Application of a stochastic model to the Q_I phase will be finished by May 2020, just before I defend my dissertation.

TABLE 1 Estimated Timeline for Completion of Objectives

August 2019	•	Complete Stochastic Model for H_{II} phase (Objective 3)
September 2019	•	Finalize Q_I phase structure (Objective 4)
January 2020	•	Finish transport study of Q_I phase (Objective 4)
April 2020	•	Finish application of stochastic model to Q_I phase (Objective 4)
May 2020	•	PhD Defense

5 Resource Requirements

The remainder of our work will require the use of high performance computing (HPC) resources. We will continue using Bridges, an XSEDE resource as well as Summit, a supercomputer located at CU Boulder.

6 Safety Considerations

Although my work is confined to computer work in an office space, there are associated health risks that I must mitigate. Proper ergonomics ensure maximum comfort and help me to work efficiently. Sitting up straight and having proper back support are necessary to relieve pressure on the discs of my vertebrae. My monitors are positioned an arm’s length directly in front of me with the tops of the monitors at eye level in order to reduce head, neck and eye strain. Finally, I take frequent breaks and go for walks around the building.

References

- ¹ C. Fritzmann, J. Lwenberg, T. Wintgens, and T. Melin, “State-of-the-Art of Reverse Osmosis Desalination,” *Desalination*, vol. 216, pp. 1–76, Oct. 2007.
- ² R. P. Schwarzenbach, B. I. Escher, K. Fenner, T. B. Hofstetter, C. A. Johnson, U. v. Gunten, and B. Wehrli, “The Challenge of Micropollutants in Aquatic Systems,” *Science*, vol. 313, pp. 1072–1077, Aug. 2006.
- ³ R. Singh, “Production of High-Purity Water by Membrane Processes,” *Desalin Water Treat*, vol. 3, pp. 99–110, Mar. 2009.
- ⁴ N. Liu, L. Li, B. McPherson, and R. Lee, “Removal of Organics from Produced Water by Reverse Osmosis Using Mfi-Type Zeolite Membranes,” *J. Membr. Sci.*, vol. 325, pp. 357–361, Nov. 2008.
- ⁵ J. R. Werber, C. O. Osuji, and M. Elimelech, “Materials for Next-Generation Desalination and Water Purification Membranes,” *Nat. Rev. Mater.*, vol. 1, p. 16018, May 2016.
- ⁶ C. M. Sales and P. K. Lee, “Resource Recovery from Wastewater: Application of Meta-Omics to Phosphorus and Carbon Management,” *Curr. Opin. Biotechnol.*, vol. 33, pp. 260–267, June 2015.
- ⁷ S. M. Dischinger, J. Rosenblum, R. D. Noble, D. L. Gin, and K. G. Linden, “Application of a Lyotropic Liquid Crystal Nanofiltration Membrane for Hydraulic Fracturing Flowback Water: Selectivity and Implications for Treatment,” *J. Membr. Sci.*, vol. 543, pp. 319–327, Dec. 2017.
- ⁸ G. L. Theodori, A. Luloff, F. K. Willits, and D. B. Burnett, “Hydraulic Fracturing and the Management, Disposal, and Reuse of Frac Flowback Waters: Views from the Public in the Marcellus Shale,” *Energy Res. Soc. Sci.*, vol. 2, pp. 66–74, June 2014.
- ⁹ B.-H. Jeong, E. M. V. Hoek, Y. Yan, A. Subramani, X. Huang, G. Hurwitz, A. K. Ghosh, and A. Jawor, “Interfacial Polymerization of Thin Film Nanocomposites: A New Concept for Reverse Osmosis Membranes,” *J. Membr. Sci.*, vol. 294, pp. 1–7, May 2007.
- ¹⁰ B. Van Der Bruggen, C. Vandecasteele, T. Van Gestel, W. Doyen, and R. Leysen, “A Review of Pressure-Driven Membrane Processes in Wastewater Treatment and Drinking Water Production,” *Environ. Prog.*, vol. 22, pp. 46–56, Apr. 2003.
- ¹¹ F. G. Donnan, “Theory of Membrane Equilibria and Membrane Potentials in the Presence of Non-Dialysing Electrolytes. a Contribution to Physical-Chemical Physiology,” *J. Membr. Sci.*, vol. 100, pp. 45–55, Mar. 1995.
- ¹² C. A. Smolders, A. J. Reuvers, R. M. Boom, and I. M. Wienk, “Microstructures in Phase-Inversion Membranes. Part 1. Formation of Macrovoids,” *J. Membr. Sci.*, vol. 73, pp. 259–275, Oct. 1992.

- ¹³ T. Humplik, J. Lee, S. C. O'Hern, B. A. Fellman, M. A. Baig, S. F. Hassan, M. A. Atieh, F. Rahman, T. Laoui, R. Karnik, and E. N. Wang, "Nanostructured Materials for Water Desalination," *Nanotechnology*, vol. 22, no. 29, p. 292001, 2011.
- ¹⁴ D. Cohen-Tanugi, L.-C. Lin, and J. Grossman, "Multilayer Nanoporous Graphene Membranes for Water Desalination," *Nano Lett.*, vol. 16, pp. 1027–1033, Jan. 2016.
- ¹⁵ Y. Wei, Y. Zhang, X. Gao, Z. Ma, X. Wang, and C. Gao, "Multilayered graphene oxide membranes for water treatment: A review," *Carbon*, vol. 139, pp. 964–981, Nov. 2018.
- ¹⁶ G. Hummer, J. C. Rasaiah, and J. P. Noworyta, "Water conduction through the hydrophobic channel of a carbon nanotube," *Nature*, vol. 414, no. 6860, pp. 188–190, 2001.
- ¹⁷ N. G. Sahoo, S. Rana, J. W. Cho, L. Li, and S. H. Chan, "Polymer nanocomposites based on functionalized carbon nanotubes," *Progress in Polymer Science*, vol. 35, pp. 837–867, July 2010.
- ¹⁸ M. Pendergast and E. M. V. Hoek, "A review of water treatment membrane nanotechnologies," *Energy & Environmental Science*, vol. 4, no. 6, pp. 1946–1971, 2011.
- ¹⁹ S. M. Auerbach, K. A. Carrado, and P. K. Dutta, eds., *Handbook of zeolite science and technology*. New York: M. Dekker, 2003. OCLC: ocm52850544.
- ²⁰ Y. Li, T.-S. Chung, and S. Kulprathipanja, "Novel Ag+-zeolite/polymer mixed matrix membranes with a high CO₂/CH₄ selectivity," *AIChE Journal*, vol. 53, no. 3, pp. 610–616, 2007.
- ²¹ M. Zhou, T. J. Kidd, R. D. Noble, and D. L. Gin, "Supported Lyotropic Liquid-Crystal Polymer Membranes: Promising Materials for Molecular-Size-Selective Aqueous Nanofiltration," *Adv. Mater.*, vol. 17, pp. 1850–1853, Aug. 2005.
- ²² M. Zhou, P. R. Nemade, X. Lu, X. Zeng, E. S. Hatakeyama, R. D. Noble, and D. L. Gin, "New Type of Membrane Material for Water Desalination Based on a Cross-Linked Bicontinuous Cubic Lyotropic Liquid Crystal Assembly," *J. Am. Chem. Soc.*, vol. 129, pp. 9574–9575, Aug. 2007.
- ²³ R. C. Smith, W. M. Fischer, and D. L. Gin, "Ordered Poly(p-phenylenevinylene) Matrix Nanocomposites via Lyotropic Liquid-Crystalline Monomers," *J. Am. Chem. Soc.*, vol. 119, no. 17, pp. 4092–4093, 1997.
- ²⁴ E. S. Hatakeyama, C. J. Gabriel, B. R. Wiesenauer, J. L. Lohr, M. Zhou, R. D. Noble, and D. L. Gin, "Water Filtration Performance of a Lyotropic Liquid Crystal Polymer Membrane with Uniform, Sub-1-Nm Pores," *J. Membr. Sci.*, vol. 366, no. 1-2, pp. 62–72, 2011.
- ²⁵ E. S. Hatakeyama, B. R. Wiesenauer, C. J. Gabriel, R. D. Noble, and D. L. Gin, "Nanoporous, Bicontinuous Cubic Lyotropic Liquid Crystal Networks via Polymerizable Gemini Ammonium Surfactants," *Chem. Mater.*, vol. 22, pp. 4525–4527, Aug. 2010.

- ²⁶ B. M. Carter, B. R. Wiesenauer, E. S. Hatakeyama, J. L. Barton, R. D. Noble, and D. L. Gin, “Glycerol-Based Bicontinuous Cubic Lyotropic Liquid Crystal Monomer System for the Fabrication of Thin-Film Membranes with Uniform Nanopores,” *Chem. Mater.*, vol. 24, pp. 4005–4007, Nov. 2012.
- ²⁷ M. Matyka, A. Khalili, and Z. Koza, “Tortuosity-Porosity Relation in Porous Media Flow,” *Phys. Rev. E*, vol. 78, p. 026306, Aug. 2008.
- ²⁸ X. Feng, M. E. Tousley, M. G. Cowan, B. R. Wiesenauer, S. Nejati, Y. Choo, R. D. Noble, M. Elimelech, D. L. Gin, and C. O. Osuji, “Scalable Fabrication of Polymer Membranes with Vertically Aligned 1 nm Pores by Magnetic Field Directed Self-Assembly,” *ACS Nano*, vol. 8, pp. 11977–11986, Dec. 2014.
- ²⁹ X. Feng, S. Nejati, M. G. Cowan, M. E. Tousley, B. R. Wiesenauer, R. D. Noble, M. Elimelech, D. L. Gin, and C. O. Osuji, “Thin Polymer Films with Continuous Vertically Aligned 1 nm Pores Fabricated by Soft Confinement,” *ACS Nano*, vol. 10, pp. 150–158, Jan. 2016.
- ³⁰ S. M. Dischinger, M. J. McGrath, K. R. Bourland, R. D. Noble, and D. L. Gin, “Effect of Post-Polymerization Anion-Exchange on the Rejection of Uncharged Aqueous Solutes in Nanoporous, Ionic, Lyotropic Liquid Crystal Polymer Membranes,” *J. Membr. Sci.*, vol. 529, pp. 72–79, May 2017.
- ³¹ R. Resel, G. Leising, P. Markart, M. Kriechbaum, R. Smith, and D. Gin, “Structural properties of polymerised lyotropic liquid crystals phases of 3,4,5-tris(-acryloxyalkoxy)benzoate salts,” *Macromol. Chem. Phys.*, vol. 201, pp. 1128–1133, July 2000.
- ³² M. O. Sinnokrot, E. F. Valeev, and C. D. Sherrill, “Estimates of the Ab Initio Limit for Interactions: The Benzene Dimer,” *J. Am. Chem. Soc.*, vol. 124, pp. 10887–10893, Sept. 2002.
- ³³ A. Gierer and K. Wirtz, “Molekulare Theorie der Mikroreibung - Molecular Theory of Microfriction,” *Z. Naturforsch.*, vol. 8, pp. 532–538, 1953.
- ³⁴ H. S. Biswal, “Hydrogen Bonds Involving Sulfur: New Insights from ab Initio Calculations and Gas Phase Laser Spectroscopy,” in *Noncovalent Forces* (S. Scheiner, ed.), Challenges and Advances in Computational Chemistry and Physics, pp. 15–45, Cham: Springer International Publishing, 2015.
- ³⁵ Y. Meroz and I. M. Sokolov, “A Toolbox for Determining Subdiffusive Mechanisms,” *Phys. Rep.*, vol. 573, pp. 1–29, Apr. 2015.
- ³⁶ Y. Meroz, I. M. Sokolov, and J. Klafter, “Subdiffusion of Mixed Origins: When Ergodicity and Nonergodicity Coexist,” *Phys. Rev. E*, vol. 81, p. 010101, Jan. 2010.
- ³⁷ C. Truong, L. Oudre, and N. Vayatis, “A Review of Change Point Detection Methods,” *arXiv*, Jan. 2018. arXiv: 1801.00718.
- ³⁸ R. Howard, *Dynamic Programming and Markov Processes*. Oxford, England: John Wiley, 1960.

- ³⁹ R. Kalman, “A New Approach to Linear Filtering and Prediction Problems,” *Journal of Basic Engineering*, 1960.
- ⁴⁰ A. Lee, K. Tsekouras, C. Calderon, C. Bustamante, and S. Press, “Unraveling the Thousand Word Picture: An Introduction to Super-Resolution Data Analysis,” *Chem. Rev.*, vol. 117, pp. 7276–7330, June 2017.
- ⁴¹ J. D. Hamilton, *Time Series Analysis*. Princeton University Press, 1994.
- ⁴² B. A. Pindzola, J. Jin, and D. L. Gin, “Cross-Linked Normal Hexagonal and Bicontinuous Cubic Assemblies via Polymerizable Gemini Amphiphiles,” *J. Am. Chem. Soc.*, vol. 125, pp. 2940–2949, Mar. 2003.
- ⁴³ J. Mondal, M. Mahanthappa, and A. Yethiraj, “Self-Assembly of Gemini Surfactants: A Computer Simulation Study,” *J. Phys. Chem. B*, vol. 117, pp. 4254–4262, Apr. 2013.
- ⁴⁴ A. D. Benedicto and D. F. O’Brien, “Bicontinuous Cubic Morphologies in Block Copolymers and Amphiphile/Water Systems: Mathematical Description through the Minimal Surfaces,” *Macromolecules*, vol. 30, pp. 3395–3402, June 1997.